DOI: http://dx.doi.org/10.1590/2179-10742019v18i21506

Quad-Band Printed Antenna for Portable WLAN Applications

Murilo H. Seko and Fatima S. Correra
Department of Electronic Systems Engineering, Polytechnic School, University of Sao Paulo
mhseko@lme.usp.br, fcorrera@lme.usp.br

***Abstract*— This paper presents a novel printed monopole antenna for quad-band operation in four WLAN bands: ISM 2.4 GHz, 5.2 GHz, 5.6 GHz, and ISM 5.8 GHz. This antenna is compact, thin, lightweight, easy to manufacture, and suitable for portable devices. It is composed of a folded strip radiator and two parasitic strips printed on a partially grounded substrate. The folded strip radiator interacts with the parasitic strips, which are connected to the ground plane, in such a way as to produce the resonant modes that originate the radiation bands of the antenna. An additional open-ended strip connected to the radiator is used to adjust the antenna input impedance in the upper operation band. A parametric study on several geometrical dimensions of the antenna is carried out in order to analyze their influence on the antenna performance. The fabricated prototype of the proposed printed monopole antenna has overall dimensions of 22 × 48 × 1.6 mm^3, and the measured 10-dB return-loss bands exhibited by the antenna are 2149–2660 MHz and 5120–6035 MHz.**

***Index Terms*—** Multiband Antennas, Portable-Device Antennas, Printed Monopole Antennas.

I. INTRODUCTION

In the last years, technology advances in the areas of microelectronics, telecommunications, and computation have enabled the development of several wireless communication systems, providing a great variety of services and applications. Additionally, the availability of smaller and cheaper devices has attracted an increasing number of users in recent times.

Because of the great and rapid popularization of mobile phone, wireless local area network (WLAN), and wireless personal area network (WPAN) systems, the use of the electromagnetic spectrum in the lower microwave frequency range, notably in the L and S bands, has become increasingly intense, favoring the occurrence of spectrum saturation and electromagnetic interference, which deteriorate the communication performance.

In order to overcome these effects and achieve higher data transfer rates, which is required by some modern applications such as video streaming and conferencing, many of the mentioned wireless communication systems have adopted additional operating bands at higher frequencies. For instance, WLAN systems in the USA and Europe have started to operate in the 5.2 GHz (5.15–5.35 GHz), 5.6 GHz (5.47–5.725 GHz), and ISM 5.8 GHz (5.725–5.850) bands, in addition to the traditional ISM 2.4 GHz (2.4–2.4835 GHz) band [1].

Various promising multiband antenna designs for portable WLAN devices are found in the

Brazilian Microwave and Optoelectronics Society-SBMO *received 24 Oct 2018; for review 1 Nov 2018; accepted 20 March 2019*
Brazilian Society of Electromagnetism-SBMag *ISSN 2179-1074*

DOI: http://dx.doi.org/10.1590/2179-10742019v18i21506

literature [2]–[10]. Some of them [2]–[4] are compact and single layered but are intended only for dual-band operation. Others [5], [6], despite their quad-band performance, display a nonplanar structure, which is more difficult to fabricate. Some other antennas [7]–[9] are able to operate in all four WLAN bands, but they require the use of a large ground plane. On the other hand, the realization of a small printed quad-band antenna for WLAN systems has been demonstrated [10].

This paper proposes a novel printed monopole antenna for quad-band operation in the ISM 2.4 GHz, 5.2 GHz, 5.6 GHz, and ISM 5.8 GHz bands. This multiband antenna is compact, low profile, lightweight, easy to fabricate, and inexpensive, meeting the requirements of portable devices [11]. The configuration and design of the antenna are presented, and the experimental results are analyzed.

II. ANTENNA CONFIGURATION

The geometry of the proposed antenna is illustrated in Fig. 1.

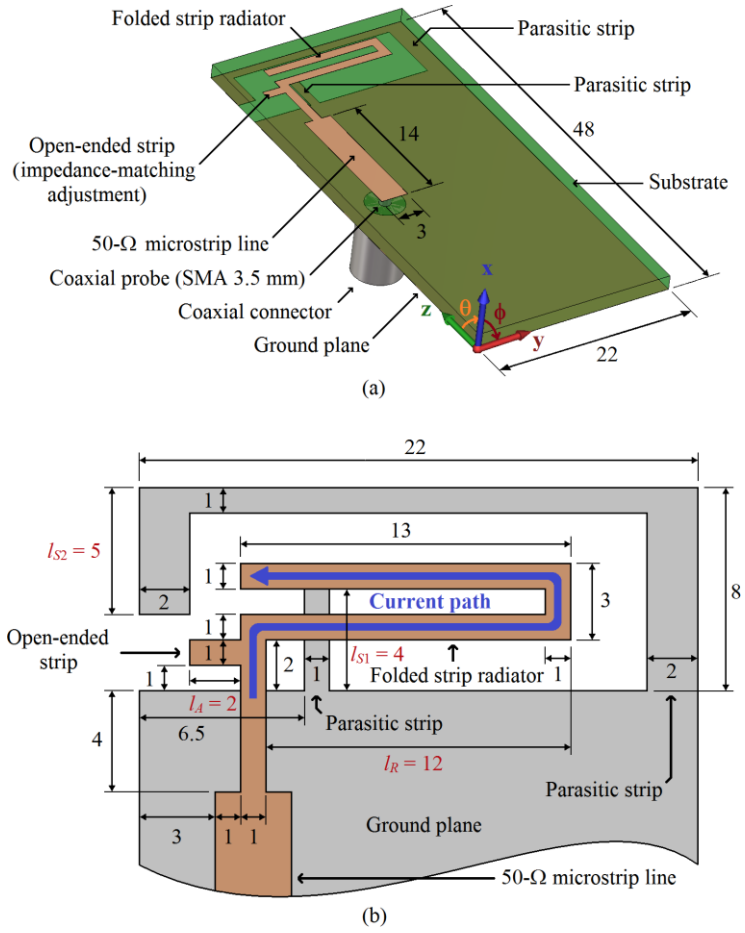

Fig. 1. Geometry of the proposed antenna: (a) perspective view of the entire antenna and (b) front view of the radiator area exhibiting both metal layers of the antenna superimposed. Dimensions are given in millimeters.

A folded strip radiator is printed on the top face of a rectangular 1.6-mm-thick FR4 substrate (dielectric constant $\varepsilon_r \approx 4.2$). The radiator is located near one of the short edges of the substrate and is

Brazilian Microwave and Optoelectronics Society-SBMO *received 24 Oct 2018; for review 1 Nov 2018; accepted 20 March 2019*
Brazilian Society of Electromagnetism-SBMag

ISSN 2179-1074

DOI: http://dx.doi.org/10.1590/2179-10742019v18i21506

connected to a 50-Ω microstrip line built on the same substrate face. A ground plane covers the bottom face of the substrate almost entirely, leaving a no-ground region under the radiator. Two parasitic strips printed on the latter substrate face (on the area that is not coated with metal) are connected to the ground plane. An open-ended strip on the top face of the substrate is connected to the radiator for adjusting the antenna input impedance in the upper operation band. The radiator, ground plane, strips, and microstrip line are built on 17-µm-thick copper layers (conductivity $\sigma = 5.8 \cdot 10^7$ S/m) covering both faces of the substrate. The antenna is fed through a 3.5-mm SMA connector mounted on the ground plane, which is connected to the microstrip line by means of a coaxial probe. The free area on the top face of the substrate can be used for the circuit of the wireless communication device in which the antenna is to be employed.

The strip radiator comprises a folded monopole, on which a linear current distribution is excited. The folded geometry of the radiator allows the current path (indicated in Fig. 1(b)) to be longer without the need for increasing the substrate size. Hence, lower operation frequencies can be achieved while maintaining a small size for the antenna. The electromagnetic field generated by the radiator excites the parasitic strips through proximity coupling, and the joint operation of all these elements leads to the resonant modes that result in the specified radiation bands.

As will be seen later in more detail, the antenna exhibits a typical return-loss curve whose behavior is represented in Fig. 2.

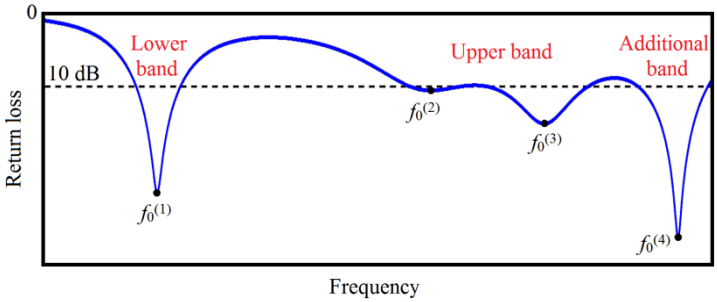

Fig. 2. Typical return-loss curve for the antenna.

Fig. 2 indicates that the resonant modes excited in the antenna lead to several peaks in the return-loss curve. The frequencies at which the first four of them occur are denoted by $f_0^{(1)}$, $f_0^{(2)}$, $f_0^{(3)}$, and $f_0^{(4)}$, in ascending order of frequency.

The resonances observed at $f_0^{(1)}$, $f_0^{(2)}$, and $f_0^{(4)}$ correspond to three different resonant modes excited on the folded monopole. The first one at $f_0^{(1)}$ is the fundamental mode. Because the strip radiator behaves as a quarter-wavelength resonant structure at this frequency, its total length L can be estimated by using the following expression:

$$L \approx \frac{\lambda_0^{(1)}}{4} = \frac{c}{4 f_0^{(1)}} \tag{1}$$

where $\lambda_0^{(1)}$ is the wavelength in free space at $f_0^{(1)}$, and c is the speed of light in vacuum. The resonant

ISSN 2179-1074

DOI: http://dx.doi.org/10.1590/2179-10742019v18i21506

modes at $f_0^{(2)}$ and $f_0^{(4)}$ are higher-order ones occurring approximately at the second and third harmonics of $f_0^{(1)}$, respectively:

$$f_0^{(2)} \approx 2\, f_0^{(1)} \tag{2}$$

$$f_0^{(4)} \approx 3\, f_0^{(1)} \tag{3}$$

Results from electromagnetic simulation indicate that the resonance at $f_0^{(3)}$ is generated by the addition of two parasitic strips to the ground plane, as shown in Fig. 1. These parasitic strips are excited by the folded radiator by means of proximity coupling. Because this excitation mechanism is somewhat complex, the evaluation of $f_0^{(3)}$ is not straightforward, and the dimensions of the parasitic strips must be obtained empirically with the aid of electromagnetic simulation.

Since the natural resonance frequencies of the monopole radiator are affected by its electromagnetic coupling with the parasitic strips, electromagnetic simulation is required for accurately analyze and design the entire antenna structure.

For the antenna design presented in this paper, the first two 10-dB return-loss bands noticeable in Fig. 2 cover all required WLAN bands: the first one (lower band) corresponds to the ISM 2.4 GHz band, and the second one (upper band) includes the 5.2 GHz, 5.6 GHz, and ISM 5.8 GHz bands. Besides that, the third 10-dB return-loss band showed in Fig. 2 (additional band) is available for receiving and transmitting signals around 6.7 GHz.

III. ANTENNA DESIGN: ANALYSIS AND OPTIMIZATION

The proposed antenna was analyzed and optimized with the aid of computer simulation, which was conducted using CST Microwave Studio, from CST Studio Suite [12], and Momentum, from Advanced Design System [13]. All simulated data exhibited in this paper resulted from CST Microwave Studio, except for the simulated surface current distribution, which was obtained using Momentum.

The performance of the antenna was studied by simulating its surface current distribution, return loss, and radiation pattern. The influence of several geometrical parameters on the characteristics of the antenna was also analyzed. Fig. 3 presents the simulated return loss of the antenna as a function of the following geometrical parameters: partial length of the radiator l_R (varied from 10 to 14 mm), length of the first parasitic strip l_{S1} (varied from 3 to 5 mm), partial length of the second parasitic strip l_{S2} (varied from 3 to 7 mm), and length of the open-ended strip l_A (varied from 0 to 4 mm). For this parametric study, l_R, l_{S1}, l_{S2}, and l_A were varied individually, keeping all other geometrical dimensions the same as given in Fig. 1.

Brazilian Microwave and Optoelectronics Society-SBMO *received 24 Oct 2018; for review 1 Nov 2018; accepted 20 March 2019*
Brazilian Society of Electromagnetism-SBMag *ISSN 2179-1074*

DOI: http://dx.doi.org/10.1590/2179-10742019v18i21506

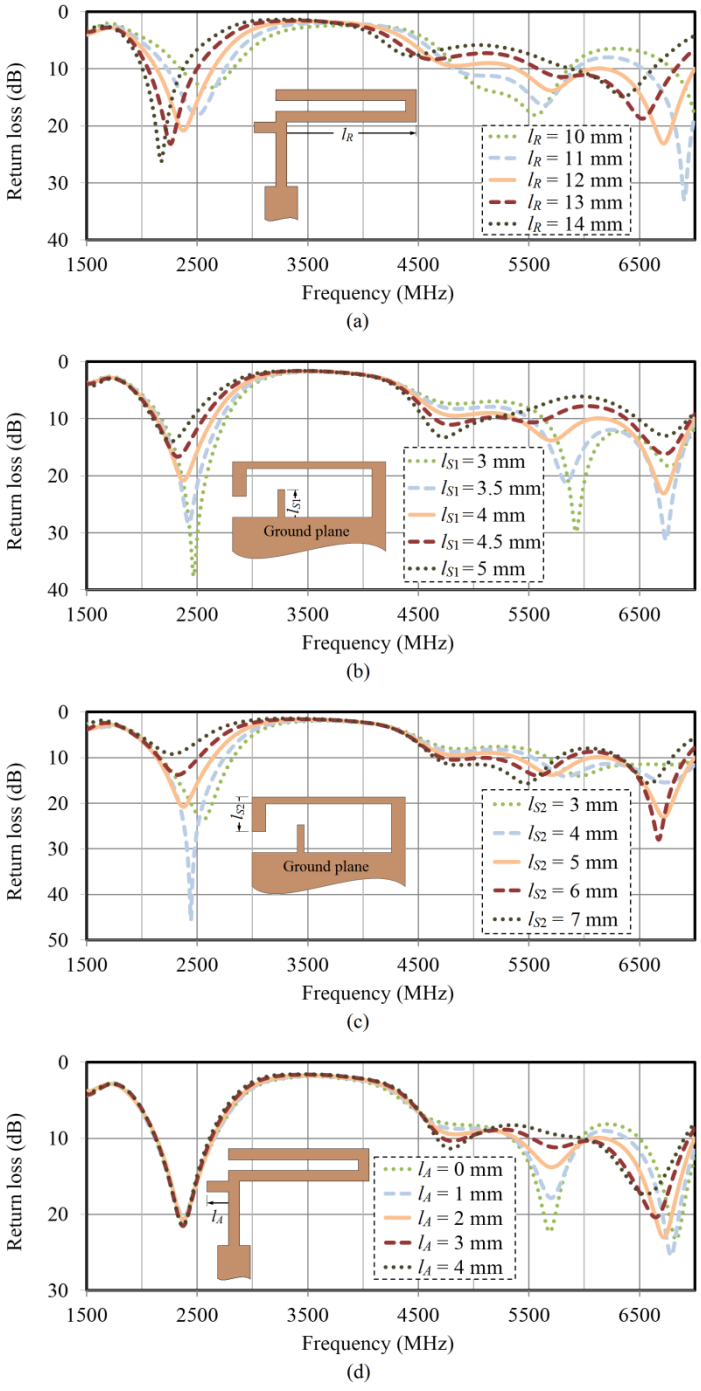

Fig. 3. Simulated return loss of the antenna as a function of (a) l_R, (b) l_{S1}, (c) l_{S2}, and (d) l_A.

One can observe from Fig. 3 that the variation of each one of the mentioned geometrical parameters has a different effect on $f_0^{(1)}$, $f_0^{(2)}$, $f_0^{(3)}$, $f_0^{(4)}$, and their corresponding return-loss level. The influence of l_R, l_{S1}, l_{S2}, and l_A on these frequencies is summarized in Table I, for which the following notation is employed: negligible change (—), slight increase (↑), slight decrease (↓), and strong decrease (↓↓).

Brazilian Microwave and Optoelectronics Society-SBMO *received 24 Oct 2018; for review 1 Nov 2018; accepted 20 March 2019*
Brazilian Society of Electromagnetism-SBMag

ISSN 2179-1074

DOI: http://dx.doi.org/10.1590/2179-10742019v18i21506

TABLE I. SIMULATED INFLUENCE OF GEOMETRICAL PARAMETERS OF THE ANTENNA ON RETURN-LOSS PEAK FREQUENCIES

Parameter	Variation range		Frequency shift			
	From	To	$f_0^{(1)}$	$f_0^{(2)}$	$f_0^{(3)}$	$f_0^{(4)}$
l_R	10 mm	14 mm	↓↓	↓↓	↑	↓↓
l_{S1}	3 mm	5 mm	↓↓	↓	↓↓	—
l_{S2}	3 mm	7 mm	↓↓	—	↓↓	↓
l_A	0 mm	4 mm	—	↓	↑	↓↓

It can be seen from Fig. 3(a) and (b) that the center frequency of the lower band can be shifted in an effective way by changing l_R or l_{S1} while maintaining acceptable values of return loss and bandwidth. It is worth pointing out that the center frequency of the upper band and the impedance matching within it are also sensitive to l_R and l_{S1}.

Fig. 3(c) indicates that a fine adjustment of the return loss in the upper band can be obtained by varying l_{S2}. Similarly to what is seen for l_R and l_{S1}, the impedance matching in the lower band and its center frequency are also affected by l_{S2}.

On the other hand, the impedance matching in the upper band can be adjusted by altering l_A without causing significant changes to the return loss in the lower band, as shown in Fig. 3(d).

Based on this parametric analysis, the geometrical dimensions of the antenna were manually optimized in order to fulfill the band requirements for quad-band WLAN operation. Fig. 1 presents the final dimensions of the antenna, obtained after the optimization process. The radiating elements of the antenna occupy an area of 22 × 8 mm^2, and the overall size of the optimized antenna, including the ground plane and feeding microstrip lines, is 22 × 48 × 1.6 mm^3, which is suitable for application in compact wireless communication devices. The simulated return loss of the optimized antenna is shown in Fig. 4 (dashed line), where the coverage of all four specified bands is visible.

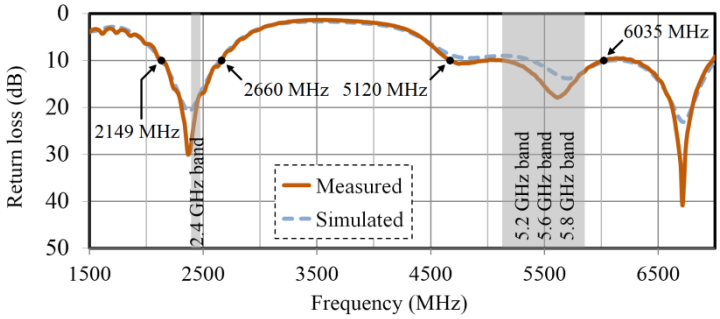

Fig. 4. Simulated and measured return loss of the antenna.

The simulated surface current distribution for the optimized antenna at 2450 and 5800 MHz is illustrated in Fig. 5.

ISSN 2179-1074

DOI: http://dx.doi.org/10.1590/2179-10742019v18i21506

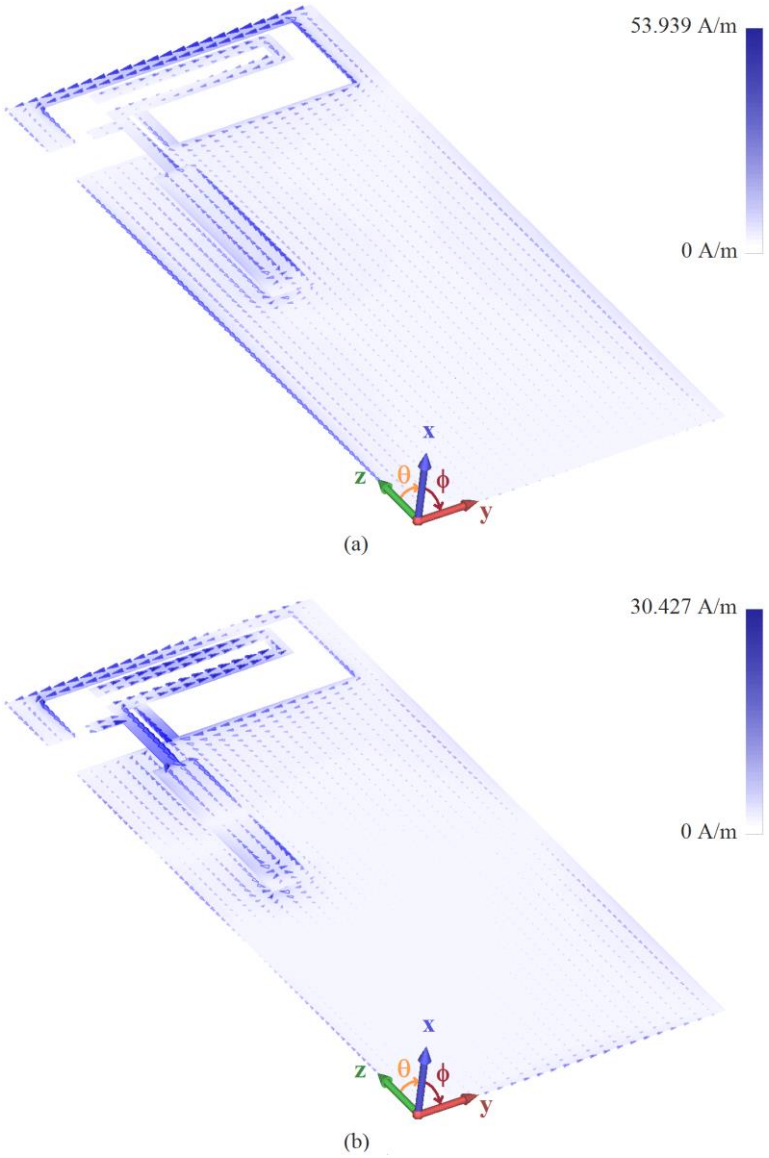

Fig. 5. Simulated surface current distribution for the antenna at (a) 2450 and (b) 5800 MHz.

For the lower-order resonant mode excited in the antenna at 2450 MHz, all current along the folded radiator points to the same direction, as shown in Fig. 5(a). At 5800 MHz, there is a change of current direction along the radiator, which can be observed in Fig. 5(b), indicating the presence of a higher-order resonant mode.

Fig. 6 presents the simulated radiation pattern of the optimized antenna at 2450 and 5800 MHz (dashed lines), showing principal plane cuts in the *xy*- and *zx*-plane (as defined in Fig. 1).

ISSN 2179-1074

DOI: http://dx.doi.org/10.1590/2179-10742019v18i21506

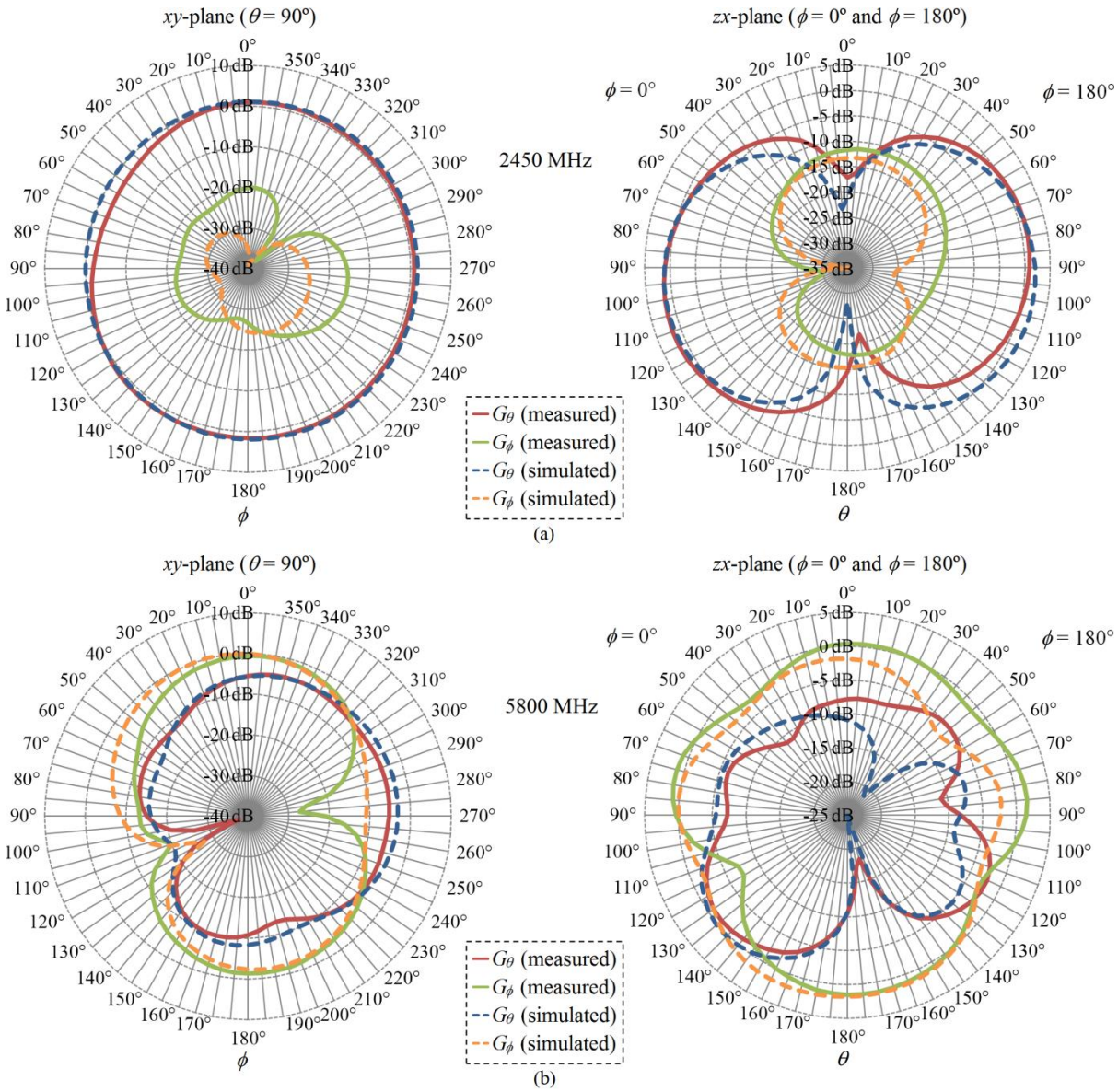

Fig. 6. Simulated and measured radiation pattern of the antenna at (a) 2450 MHz and (b) 5800 MHz.

At 2450 MHz, the antenna exhibits a dipole-like omnidirectional radiation pattern for linear polarization in the θ-direction. In general, at this same frequency, the radiation pattern shows reasonably lower gain levels for linear polarization in the ϕ-direction compared to the values observed for linear polarization in the θ-direction. Considering the radiation pattern presented by the antenna at 5800 MHz, the gain levels for linear polarization in the ϕ-direction are, on average, higher than those for linear polarization in the θ-direction, which indicates a polarization change. Table II lists the results for simulated maximum gain of the antenna, obtained from Fig. 6.

ISSN 2179-1074

DOI: http://dx.doi.org/10.1590/2179-10742019v18i21506

TABLE II. SIMULATED AND MEASURED MAXIMUM GAIN OF THE ANTENNA

Frequency (MHz)	Gain (dB)							
	xy-plane				*zx*-plane			
	Meas. G_θ	Sim. G_θ	Meas. G_ϕ	Sim. G_ϕ	Meas. G_θ	Sim. G_θ	Meas. G_ϕ	Sim. G_ϕ
2450	1.8	2.2	-15	-23	1.7	2.2	-11	-13
5800	-4.5	-3.0	-0.54	0.14	-0.73	0.27	1.6	1.9

For the sake of completeness, Fig. 7 and 8 display simulated results for the antenna at 6720 MHz, which is the frequency at which the fourth return-loss peak occurs ($f_0^{(4)}$), with reference to Fig. 2. Fig. 7 exhibits the surface current distribution, and Fig. 8 shows the radiation pattern.

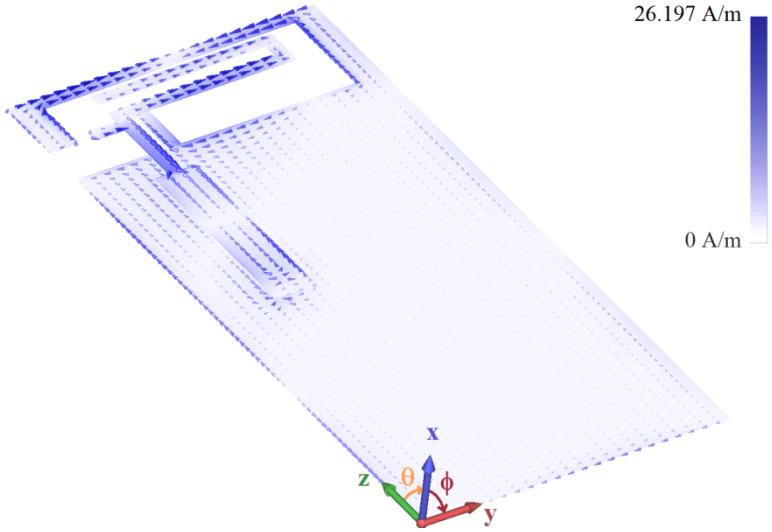

Fig. 7. Simulated surface current distribution for the antenna at 6720 MHz.

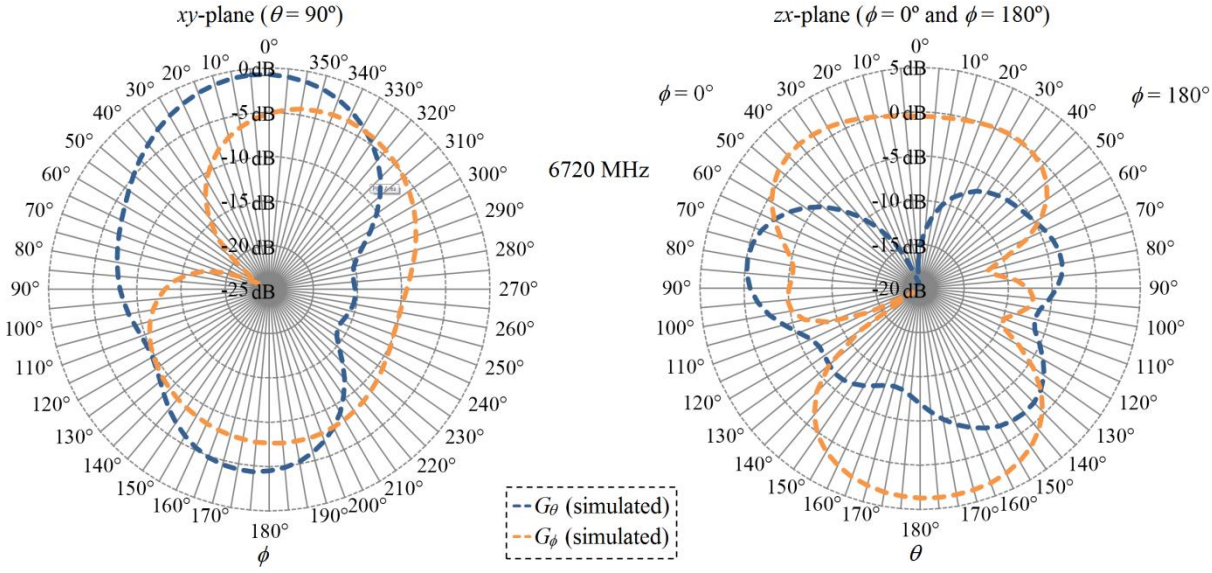

Fig. 8. Simulated radiation pattern of the antenna at 6720 MHz.

ISSN 2179-1074

DOI: http://dx.doi.org/10.1590/2179-10742019v18i21506

IV. EXPERIMENTAL RESULTS

A prototype of the optimized antenna was fabricated using a micro-milling machine. Photographs of the fabricated prototype are presented in Fig. 9, displaying both sides of the antenna.

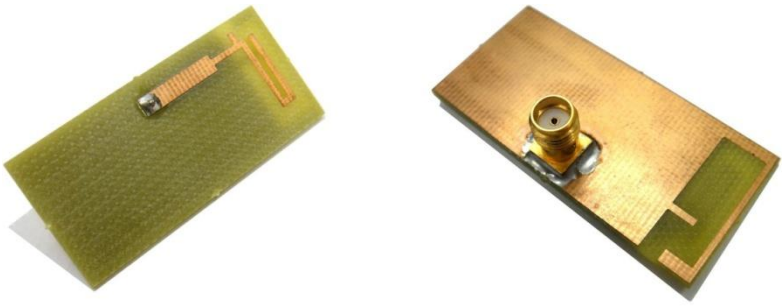

(a) (b)

Fig. 9. Fabricated antenna prototype: (a) front and (b) back view.

The measured return loss of the antenna, obtained by using a network analyzer, is shown in Fig. 4 along with the corresponding simulated results. Both simulated and measured return-loss curves demonstrate a good agreement with each other, as can be seen in Fig. 4. The experimental 10-dB return-loss bands are 2149–2660 MHz and 5120–6035 MHz, which include all required WLAN bands.

The fabricated prototype was characterized in an anechoic chamber. Fig. 6 exhibits the measured results for the radiation pattern of the antenna along with their respective simulated data.

The agreement between the experimental and simulated results for radiation pattern shown in Fig. 6 and Table II suggests that the antenna has a radiation performance close to that predicted by simulation.

V. CONCLUSION

A compact printed monopole antenna for quad-band operation in four WLAN bands has been developed. In this antenna, the radiation bands are generated by the excitation of multiple resonant modes. The proposed antenna configuration was studied, and its geometry was optimized in order to meet the design specifications. An investigation into the structure and performance of this antenna using electromagnetic simulation demonstrates that the center frequencies of its operation bands can be tuned by adjusting a few geometrical dimensions. A prototype of the proposed printed monopole antenna was fabricated and characterized. The overall dimensions of the antenna are $22 \times 48 \times 1.6\ mm^3$, and its experimental 10-dB return-loss bands are 2149–2660 MHz and 5120–6035 MHz. The measured radiation pattern of the antenna shows maximum gain of 1.8 dB at 2450 MHz and 1.6 dB at 5800 MHz, for linear polarization on its principal cut planes. A good agreement is observed between the experimental and simulated results, validating the proposed antenna configuration. These results demonstrate the realization of a compact, thin, and

Brazilian Microwave and Optoelectronics Society-SBMO *received 24 Oct 2018; for review 1 Nov 2018; accepted 20 March 2019*
Brazilian Society of Electromagnetism-SBMag *ISSN 2179-1074*

DOI: http://dx.doi.org/10.1590/2179-10742019v18i21506

easy-to-fabricate antenna that can operate in four WLAN bands. This antenna employs a small radiator and can be easily integrated with circuits, making it attractive for use in portable wireless communication devices such as mobile phones, tablets, laptops, WLAN dongles, and WLAN routers.

ACKNOWLEDGMENT

This work was supported by National Council for Scientific and Technological Development, Brazil (CNPq). The authors also gratefully thank University of Houston, USA for providing the anechoic chamber used for the measurements of the antenna.

REFERENCES

[1] D. A. Sanchez-Hernandez, *Multiband integrated antennas for 4G terminals*. Norwood, MA, USA: Artech House, 2008.
[2] C.-M. Su, H.-T. Chen, F.-S. Chang, and K.-L Wong, "Dual-band slot antenna for 2.4/5.2 GHz WLAN operation," *Microwave Opt. Technol. Lett.*, vol. 35, no. 4, pp. 306–308, Nov. 2002.
[3] J. Jung, H. Lee, and Y. Lim, "Compact monopole antenna for dual ISM-bands (2.4 and 5.8 GHz) operation," *Microwave Opt. Technol. Lett.*, vol. 51, no. 9, pp. 2227–2229, Sep. 2009.
[4] Y. Li, W. Li, and Q. Ye, "A compact asymmetric coplanar strip-fed dual-band antenna for 2.4/5.8 GHz WLAN applications," *Microwave Opt. Technol. Lett.*, vol. 55, no. 9, pp. 2066–2070, Sep. 2013.
[5] Y. J. Cho, Y. S. Shin, and S.-O. Park, "Dual-band internal WLAN antenna for 2.4/5 GHz laptop PC applications," *Microwave Opt. Technol. Lett.*, vol. 48, no. 11, pp. 2349–2354, Nov. 2006.
[6] C.-T. Lee and S.-W. Su, "Very-low-profile, 2.4/5.2/5.8-GHz, triband WLAN antenna for laptop-tablet computer with complete metal cover," *Microwave Opt. Technol. Lett.*, vol. 58, no. 1, pp. 225–233, Jan. 2016.
[7] Y.-S. Liu, J.-S. Sun, R.-H. Lu, and Y.-J. Lee, "New multiband printed meander antenna for wireless applications," *Microwave Opt. Technol. Lett.*, vol. 47, no. 6, pp. 539–543, Dec. 2006.
[8] S.-J. Liao, K.-L. Wong, and L.-C. Chou, "Small-size uniplanar coupled-fed PIFA for 2.4/5.2/5.8 GHz WLAN operation in the laptop computer," *Microwave Opt. Technol. Lett.*, vol. 51, no. 4, pp. 1023–1028, Apr. 2009.
[9] K.-L. Wong and W.-J. Chen, "Small-size microstrip-coupled printed PIFA for 2.4/5.2/5.8 GHz WLAN operation in the laptop computer," *Microwave Opt. Technol. Lett.*, vol. 51, no. 9, pp. 2072–2076, Sep. 2009.
[10] X. L. Sun, S. W. Cheung, and T. I. Yuk, "A compact monopole antenna for WLAN applications," *Microwave Opt. Technol. Lett.*, vol. 56, no. 2, pp. 469–475, Feb. 2014.
[11] R. Waterhouse, *Printed Antennas for Wireless Communications*, Chichester, England: John Wiley & Sons, 2007.
[12] CST Studio Suite 2010, CST Computer Simulation Technology AG, Darmstadt, Germany, 2010.
[13] Advanced Design System 2009, Agilent Technologies Inc., Palo Alto, CA, USA, 2010.

Brazilian Microwave and Optoelectronics Society-SBMO *received 24 Oct 2018; for review 1 Nov 2018; accepted 20 March 2019*
Brazilian Society of Electromagnetism-SBMag *ISSN 2179-1074*